Journal of Thermal Analysis and Calorimetry (2025) 150:1275–1288
https://doi.org/10.1007/s10973-024-13569-8

Interaction of an anticancer oxygenated propenylbenzene derivatives with human topoisomerase II *α* and actin: molecular modeling and isothermal titration calorimetry studies

Joanna Grzelczyk[1] · Horacio Pérez-Sánchez[2] · Jochem Nelen[2] · Miguel Carmena-Bargueño[2] · Ilona Gałązka-Czarnecka[1] · Grażyna Budryn[1] · Dawid Hernik[3] · Elisabetta Brenna[4] · Filip Boratyński[3]

Received: 1 October 2023 / Accepted: 4 August 2024 / Published online: 2 September 2024

Abstract

Cancer diseases are one of the most common causes of death. It is important to reduce the proliferation of cancer cells at an early stage, but also to limit their migration. There is a need to find new compounds of moderate anticancer prevention activity for long administration. TOPIIα and actin are proteins that in states of inflammation can cause the progression of cancer and neoblastic cell migrations. Looking for compounds that will work comprehensively in preventing cancer, interacting with both TOPIIα and actin is crucial/was our aim. In this study, the antioxidant properties of propenylbenzene derivatives and their affinity to bind actin and TOPIIα causing inhibition of their functions were evaluated. The ligand–protein binding assay was carried out by isometric titration calorimetry (ITC), and molecular docking, and the antioxidant potential. The highest chelation activity was shown by 5b: 83.95% (FRAP 18.39 µmol Fe(II) mL^{-1}). High affinity for actin and TOPIIα using ITC and docking was shown by diol forms. For actin the best ligands were 2b ($\Delta H -51.49$ kJ mol^{-1}, $\Delta G -27.37$ kJ mol^{-1}) and 5b ($\Delta H -17.25$ kJ mol^{-1}, $\Delta G -26.20$ kJ mol^{-1}), whereas for TOPIIα: 3b ($\Delta H -163.86$ kJ mol^{-1}, $\Delta G -34.60$ kJ mol^{-1}) and 5b ($\Delta H -160.93$ kJ mol^{-1}, $\Delta G -32.92$ kJ mol^{-1}). To confirm the occurrence of the interactions at the active site of the proteins, molecular docking and subsequent molecular dynamics simulations were performed, which showed for both actin and TOPIIα the highest enthalpy of interactions of 5b: -34.94 kJ mol^{-1} and -25.52 kJ mol^{-1}, respectively.

Keywords Actin polymerization · TOPII · Docking simulation · Propenylbenzenes · Antioxidant activity · ITC

✉ Joanna Grzelczyk
joanna.grzelczyk@p.lodz.pl

Horacio Pérez-Sánchez
hperez@ucam.edu

Jochem Nelen
jnelen@ucam.edu

Miguel Carmena-Bargueño
mcarmena@ucam.edu

Ilona Gałązka-Czarnecka
ilona.galazka-czarnecka@p.lodz.pl

Grażyna Budryn
grazyna.budryn@p.lodz.pl

Dawid Hernik
dawid.hernik@upwr.edu.pl

Elisabetta Brenna
mariaelisabetta.brenna@polimi.it

Filip Boratyński
filip.boratynski@upwr.edu.pl

[1] Faculty of Biotechnology and Food Sciences, Institute of Food Technology and Analysis, Lodz University of Technology, 90-537 Lodz, Poland

[2] Structural Bioinformatics and High-Performance Computing Research Group (BIO-HPC), Computer Engineering Department, Universidad Católica de Murcia (UCAM), 30107 Guadalupe, Murcia, Spain

[3] Department of Food Chemistry and Biocatalysis, Wrocław University of Environmental and Life Sciences, 50-375 Wrocław, Poland

[4] Dipartimento Di Chimica, Materiali Ed Ingegneria Chimica "Giulio Natta", Politecnico Di Milano, Milan, Italy

Introduction

Cancer diseases are the second leading cause of death in the world. Cancer cells differentiate and spread in an uncontrolled way in the human body. There are many types of cancer, and most of them are still unknown or newly discovered [1]. The strategy of cancer treatment is still developing; unfortunately, with the emergence of more and more new cases, the disease is insurmountable. It is estimated that in 2018, over 9 million people worldwide died from various types of cancer [2]. The formation of cancer cells can occur in different ways. One reason is the accumulation of reactive oxygen species (ROS). The accumulation of ROS affects the disruption of the proper functioning of tissues. This process results in the formation of oxidative stress, which causes, among others, to DNA damage, oxidizes proteins, which activates oncogenic pathways [3]. According to in vitro and in vivo studies, ROS are involved in all phases of tumor formation (phases of initiation, promotion and progression) [4]. Topoisomerase II α (TOPIIα) is an isoform of human topoisomerase II; its main task is cells proliferation; it reduces torsional stress; and it is required for the proper functioning of chromosomes (condensation, cohesion and segregation) [5, 6]. DNA double-strand breaks are catalyzed by TOPIIα, followed by induction of mitosis gene transcription [6, 7]. However, high levels of aberrant TOPIIα expression have been detected in various types of tumors.

Although there are different mechanisms of tumor formation, it is important to prevent metastasis. The main protein responsible for the migration of cancer cells and the resulting metastasis is actin, which polymerizes when malfunctioning. Actin is a structural protein. In cells, it mainly performs the function of vesicle transport, migration and cell division [8]. The actin cytoskeleton is changed during tumor metastasis. These changes occur during the transformation process due to the binding of proteins to actin. The main mechanism of changes in the actin cytoskeleton is the downregulation of several isoforms of tropomyosin. This is due to the deregulation of actin binding protein leading to actin filament dynamics [9, 10]. The dynamics of the actin filament depends on the binding to the subunits; the ADP-actin subunit dissociates faster than the ATP-actin. Activation of the complex of actin-related proteins 2 and 3 (Arp2/3) by binding to the side of the actin filament produces further branches affecting the formation of membrane sprouts, as well as cell motility, e.g. lamellipodia, filopodia [11]. In addition, cellular pseudopods are formed, the main structure of which are protuberances connected by actin. The protuberances are arranged in the direction of the movement of the cells, adjacent to its membrane. Proteins associate mainly in the VAC region, consisting of a viologen structural domain (at the C-terminus), a cophilin domain and an acid domain. Activation of the Arp2/3 complex by the VCA region results in pseudocell formation, invasion, and migration of tumor cells [12, 13]. Therefore, it is important to look for compounds that will work comprehensively in preventing cancer, interacting with both TOPIIα and actin.

In this study, the use of newly obtained propenylbenzene derivatives (diols and hydroxy ketones) by environmentally friendly methods was proposed. Propenylbenzenes have anticancer properties, so it was decided to test their derivatives. The aim of the study was to evaluate the binding of propenylbenzene derivatives to actin and TOPIIα using the methods of isothermic titration calorimetry and molecular docking and molecular dynamics, as well as to evaluate the antioxidant properties of the compounds.

Material and methods

Materials and reagents

Prop-1-en-1-yl benzene, anethole, 1,2-dimethoxy-4-prop-1-en-1-yl benzene, isoeugenol, actin from porcine muscle ~ 90% lyophilized powder containing Tri, topoisomerase II α human, 3-caffeoylqunic acid (≥ 99%), 6-Hydroxy-2,5,7,8-tetramethylchroman-2-carboxylic acid (Trolox), 2,4,6-tri(2-pyridyl)-s-triazine (TPTZ), sodium acetate, ferric chloride hexahydrate, ferrozine, and ammonium acetate were purchased from Sigma-Aldrich Chemical Co. (St. Louis, MO, USA). All other reagents were of analytical grade and were purchased from Chempur (Piekary Slaskie, Poland).

The synthesis of diols and hydroxy ketones has been described in a previous paper [14]. In short, the chemoenzymatic synthesis to obtain a mixture of two racemic diastereomers of diols was performed. Prop-1-en-1-yl benzene (2a), anethole (3a), 1,2-dimethoxy-4-prop-1-en-1-yl benzene (4a), and isoeugenol (5a) were dissolved in EtOAc (2.96 mmol/15 mL); then, 382 µL of H_2O_2 4.44 mmol and 10 mg of Novozym 435 were added. The reaction mixtures were incubated in a thermoshaker (30 °C, 18 h). After incubation, the enzyme was filtered off and the reaction was stopped by adding Na_2SO_3, and then with a saturated solution of $NaHCO_3$. The remaining fraction was dried with Na_2SO_4, concentrated under reduced pressure, and then dissolved in 15 mL of MeOH. In the next step, excess of KOH was added and left for 24 h at room temperature with continuous stirring. The resulting mixture was reduced under pressure and then diluted with H_2SO_4 solution. The resulting phase was then dried with Na_2SO_4 and concentrated. The following diols were obtained: 2a → 1-phenylpropane-1,2-diol (2b), 3a → 1-(4-methoxyphenyl)propane-1,2-diol (3b), 4a → 1-(3,4-dimethoxyphenyl)propane-1,2-diol (4b),

and 5a → 1-(4-hydroxy-3-methoxyphenyl)propane-1,2-diol (5b). The hydroxy ketones were obtained by biotransformation. The PCM medium was sterilized (121 °C for 15 min) and then inoculated with a bacterial culture (5 mL, OD_{600} = 0.3–0.5) and incubated with shaking (22 °C, 3 days). Then, diols, previously dissolved in DMSO (0.2 g/5 mL), were added to the culture. Microbial oxidation was carried out from 3 to 11 days. The following hydroxy ketones were obtained: 2b → 2-hydroxy-1-phenylpropan-1-one (2c), 3b → 2-hydroxy-1-(4-methoxyphenyl)propan-1-one (3c), 4b → 1-(3,4-dimethoxyphenyl)-2-hydroxypropan-1-one (4c).

Ferric reducing antioxidant power assay (FRAP)

The ferric reducing antioxidant potential (FRAP) test was conducted to determine the total antioxidant capacity [15, 16]. For that reason 10 µL (10 mmol) of compounds` extracts were mixed with 4 mL of FRAP. The FRAP solution was prepared by mixing 25 mL of acetate buffer (pH 3.6, 300 mmol L^{-1}) with 2.5 mL of 2,4,6-Tris(2-pyridyl)-s-triazine (TPTZ, 10 mmol L^{-1}) at 40 mmol L^{-1} HCl and 2.5 mL $FeCl_3 \cdot 6H_2O$ (20 mmol L^{-1}), the mixture was incubated in the dark (30 min, 37 °C), and the solution was mixed and incubated without the access of light (30 min, 37 °C). The absorbance was measured at 593 nm and compared with ferrous sulfate to make a standard curve. The FRAP value was shown as µmol Fe(II) mL^{-1}.

Chelating activity of Fe^{2+}

The Fe^{2+} chelating ability was determined as described previously [15]. Briefly, tested compounds (1 mL) were placed in a 20 mL vial and suitably diluted with ethanol and subsequently 100 µL of 2 mmol L^{-1} $FeCl_2$ and 4.7 mL of high-purity deionized water was added. Then, the solution was mixed for 30 s and 200 µL of 5 mmol L^{-1} ferrozine solution was added. The mixture was mixed vigorously and incubated at room temperature for 15 min. The absorbance was measured spectrophotometrically at 562 nm. A control sample was prepared by adding 5.7 mL of deionized water, 100 µL of 2.0 mmol L^{-1} $FeCl_2$ solution and mixing vigorously. After 30 s, 200 µL of a 5 mmol L^{-1} ferrozine solution was added. The sample was mixed vigorously and incubated for 15 min in a dark place. The results are expressed as the percentage chelating activity (%).

Isothermal titration calorimetry

Thermodynamic parameters of actin or TOPIIα binding to propenylbenzene derivatives were performed by isothermal titration calorimetry (ITC) using a MicroCal PEAQ-ITC200 apparatus (Malvern, Worcestershire, UK) as described previously [17]. During the ITC assay, measuring cell of the 0.2 mL was filled with degassed actin solution (100 µmol L^{-1}) or TOPIIα (100 µmol L^{-1}) and titrated with each of 2a–5a, 2b–5b and 2c–4c at a concentration of 10 mmol L^{-1}. The injection in 11 intervals was repeated 15 times at 36.6 °C with constant stirring 307 rpm and intervals between injections of 150 s. The enzyme and compounds were prepared in methanol LCMS, pH 7.6. Data were analyzed using the MicroCal PEAQ-ITC Analysis software; ''One Set of Sites'' fitting model (stoichiometry, equilibrium dissociation constant, enthalpy changes). The heat of dilution of the titrant was measured and considered during the analysis. The thermodynamic parameters (K, ΔH) calculated based on ITC data are so-called conditional (observed) parameters as their values depend on the pH of a solution and the type of the buffer used (i.e., the enthalpy buffer ionization) [18]. Before analysis, the equipment was calibrated according to the device procedures (MICROCAL PEAQ-ITC SYSTEM, Getting Started Booklet, Malvern Instruments). The run parameters for the method 19 injections. T = 20 °C. The calibration suitable for the $CaCl_2$/EDTA titration experiment. The concentrations for the syringe Syr (M) = $1e^{-3}$ ($CaCl_2$) and the Cell (M) = $100e^{-6}$ (EDTA). The sample cell with sample solution EDTA was filled, waited 2 min, emptied and refilled. The fresh water is in the reference cell (distilled water).

Molecular docking

Actin

In order to gain better insights into the binding interactions, molecular docking calculations were performed with LeadFinder [19]. For the protein structure, the actin structure with PDB code 1WUA was used. Firstly, the ligands, water molecules and metal ions were removed. Subsequently, the structure was preprocessed using Maestro's Protein Preparation Wizard [20] by adding hydrogens, (re)assigning bond orders and adding missing residue atoms. After this, the protein structure was charged using Maestro's system builder and the OPLS3e [21] forcefield and saved using the mol2 format. To obtain the smiles codes of the ligands, they were first drawn using PubChem Sketcher V2.4 [22]. The smiles were converted to SDF format using RDKit [22]. Finally, molconvert [24], part of the ChemAxon's Marvin suite, was used to convert the SDF to mol2 format using the mmff94 forcefield.

As mentioned earlier, LeadFinder was used to perform the docking. For this, the default parameters were kept, and the ATP binding site was used as the docking location. The docking pose was used as a starting position for subsequent 100 ns molecular dynamics (MD) simulations.

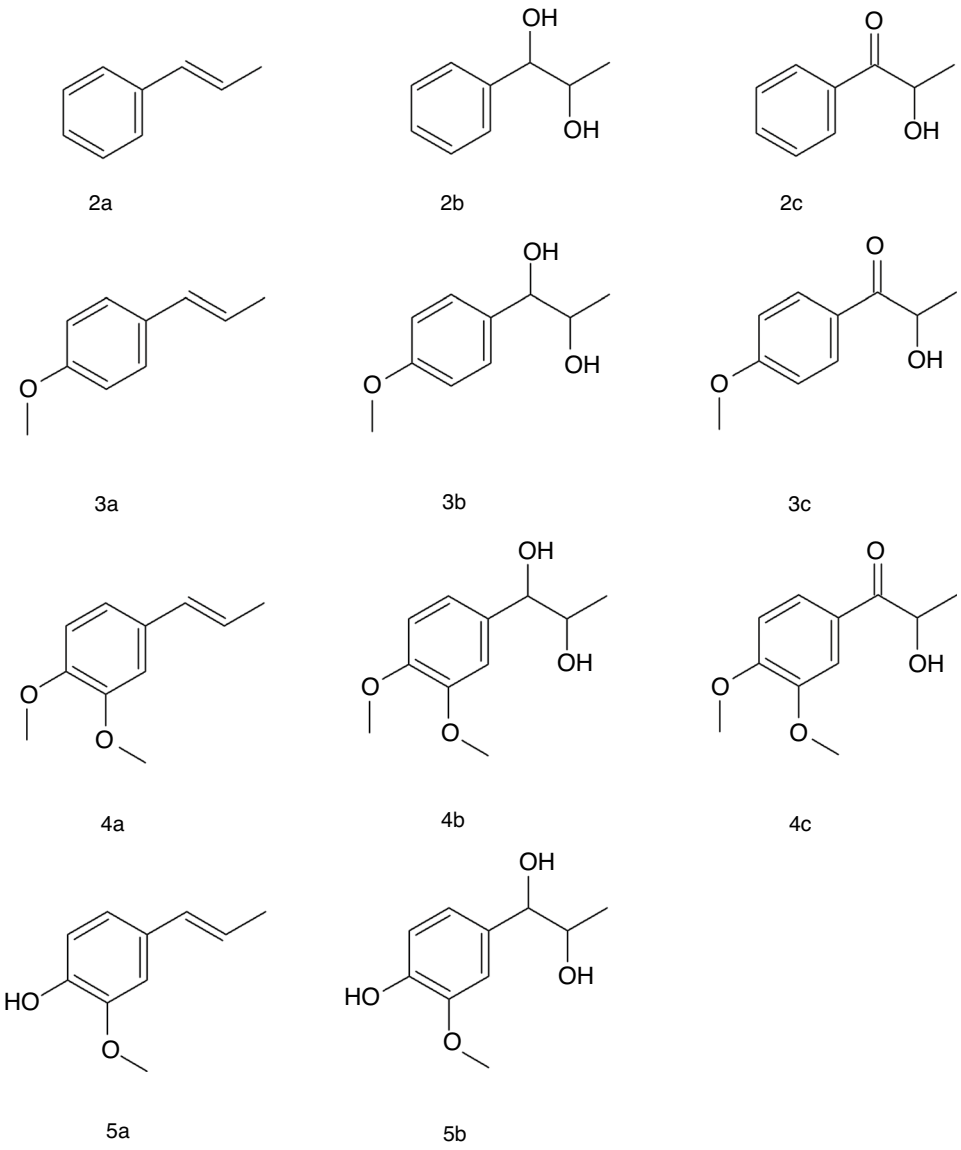

Fig. 1 Structures of the propenylbenzenes 2a–5a, diols 2b–5b and hydroxy ketones 2c–4c

TOPIIα

The analysis was performed according to the previous method with modifications [25]. Three-dimensional X-ray crystal structure of human DNA topoisomerase II, alpha isoenzyme (PDB ID 1zxm, resolution = 1.87 Å, Chains: A, B) was downloaded from the protein data bank (PDB; http://www.rcsb.org/pdb). In the first stage, a full atom model of the enzyme was prepared by calculating the ionizable amino acids' pKa values and protonation states. Then, hydrogen atoms were added, and the cap termini were included with the Protein Preparation Wizard (Maestro). The charges of the atoms of the protein were added using System Builder (Maestro). The chemical structures of all compounds (propenylbenzene derivatives) were built up manually, and partial charges were calculated as previously reported to be used during docking simulations [26]. The docking of bioactive compounds to the prepared enzyme structure model was performed using the default configuration parameters (LeadFinder docking software). The ATP binding site of TOPIIα served as the target location for molecular docking. The output docked pose was employed as the starting point for subsequent 100 ns MD simulations.

Molecular Dynamics

After the LeadFinder docking calculations, molecular dynamics (MD) simulations were performed using Maestro-Desmond implemented by Schrödinger [27, 28] to gain further insights into the protein–ligand interactions. The LeadFinder ligand–protein complexes were used as initial structures for the MD simulations. For preprocessing, the protein Maestro's preparation wizard was used to add missing hydrogens and side chains. Subsequently, the complexes

were charged with the OPLS3e force field [29] using Maestro's system builder. To ensure an accurate representation of the system, the ligand–protein complexes were immersed in an SPC (simple point charge) water box, with a buffer extending 10 Å beyond the complex's atoms to prevent the protein from leaving the water box. To replicate physiological conditions, 0.15 M NaCl was added to the solution. Furthermore, if the net charge of the system was nonzero, additional Na^+ or Cl^- ions were automatically included to neutralize the total system charge. The MD simulations were performed under constant temperature (300 K) and pressure (1 atm) conditions, utilizing the NPT ensemble to maintain a constant number of particles throughout the simulation. The OPLS3e force field was employed for all simulations. The protein–ligand complex was simulated for 100 ns in each case, with data recorded every 4.8 ps. Plots and figures depicting the simulations were generated using Maestro's Desmond simulation interaction diagram tool.

Statistical analysis

The results were expressed as mean ± standard error of the mean, n = 3. All calculations were evaluated for significance using one-way ANOVA followed by Dunnett's test with the GraphPad Prism 6.0 software (GraphPad Software, Inc., La Jolla, CA, USA). Significance was defined at $p \leq 0.05$.

Results

In our recent studies, a two-step chemo-enzymatic method for obtaining oxygenated derivatives of commercially available propenylbenzenes 2a-5a was developed [14]. The first step involves the synthesis of corresponding diols 2b-5b from propenylbenzenes 2a-5a via lipase catalyzed epoxidation followed by epoxide hydrolysis (Fig. 1). In the second step, the microbial oxidation of diols 2b-5b yielded the corresponding hydroxy ketones 2c-4c. All obtained compounds were tested for various biological activities, among them antioxidant and anticancer activities. Several compounds showed high activity; therefore, we decided herein to explore deeper their properties.

Table 1 Antioxidant properties determined by FRAP and chelating activity Fe^{2+} of propenylbenzene derivatives

Compound	FRAP/μmol Fe(II) mL^{-1}	Fe(II) chelating ability/%
2a	13.01 ± 0.59[a]	81.29 ± 0.55[a]
2b	33.05 ± 1.09[b]	69.22 ± 1.45[b]
2c	41.24 ± 1.15[c]	79.45 ± 0.59[c]
3a	3.89 ± 0.49[d]	75.08 ± 1.08[d]
3b	4.97 ± 0.55[d]	70.62 ± 1.05[d]
3c	6.14 ± 0.25[e]	81.11 ± 0.95[a]
4a	15.13 ± 0.35[a]	64.15 ± 0.87[b]
4b	25.55 ± 0.45[c]	55.11 ± 0.55[e]
4c	31.60 ± 1.15[b]	59.36 ± 0.35[e]
5a	9.11 ± 0.39[e]	69.21 ± 0.39[b]
5b	18.39 ± 0.55[a]	83.95 ± 1.05[a]

Data are shown as mean ± standard deviation, n = 3, and values followed by different superscript letters (a–e) in the same column are significantly different ($p < 0.05$).

Antioxidant potential of propenylbenzene derivatives

In a previous study, we analyzed antiradical activity using the DPPH method; however, this method only identifies the most reactive compounds [14]. The FRAP test is more accurate and covers the majority of antioxidant components; therefore, the antioxidant capacity of the tested compounds was determined using the FRAP technique. The highest activity was shown for propenylbenzenes, followed by diols and hydroxy ketones (Table 1).

The highest antioxidant potential was shown by 3a 3.89 μmol Fe(II) mL^{-1}, followed by 3b 4.97 and 3c 6.14 μmol Fe(II) mL^{-1}, and the lowest by 2c 41.24 μmol Fe(II) mL^{-1}. In the second test 5b showed the highest metal chelating activity: 83.95%. The remaining values of the chelating effect (%) were in the order as follows: 2a 81.29% > 3c 81.11% > 2c 69.22% > 3a 75.08% > 3b 70.62% > 2b 69.22% > 5a 69.21% > 4a 64.15% > 4c 59.36% > 4b 55.11%.

ITC analysis of propenylbenzene derivatives interactions

The parameters of propenylbenzene derivatives binding to actin were determined using the ITC technique. Studies have shown that for actin, the binding constant (K_a) of propenylbenzene derivatives ranged from 2.97 to 55.01×10^3 L mol^{-1}. A high actin binding constant was determined for 2a, 2b and 4c, amounting $55.01^{*}10^3$, 41.32×10^3, 34.60×10^3 L mol^{-1}, respectively, while 3b and 3c showed a lower binding constant of 2.97×10^3 and 3.24×10^3 L mol^{-1}, respectively (Table 2).

Direct titration of the tested compounds into the actin solution gave an exothermic energetic effect, which was confirmed by negative changes in the reaction enthalpy (ΔH). The ΔH range results from −51.49 to −0.71 kJ mol^{-1}, for 2b and 2a, respectively. It was observed from the data that the binding stoichiometry of the tested compounds to actin was 1:1; therefore, the data were fitted to a single-site binding reaction model. The highest negative free energy of −28.11 and −27.37 kJ mol^{-1} (ΔG) interpreted as the substances affinity for binding was recorded for 2a and 2b,

Table 2 Thermodynamic parameters of interactions between TOPIIα/actin and propenylbenzene derivatives

Compound	K_d/μmol L^{-1}	$K_a \times 10^3$/L mol^{-1}	ΔH/kJ mol^{-1}	ΔG/kJ mol^{-1}	ΔS/J mol^{-1} K^{-1}	ΔG predicted/kJ mol^{-1}
ACTIN						
2a	18.18 ± 0.01^{a}	55.01 ± 0.35^{a}	-0.71 ± 0.01^{a}	-28.11 ± 0.02^{a}	88.46 ± 0.49^{a}	−21.92
2b	24.20 ± 0.92^{b}	41.32 ± 0.49^{b}	-51.49 ± 1.98^{b}	-27.37 ± 0.03^{b}	-77.87 ± 0.18^{b}	−26.06
2c	88.20 ± 1.37^{c}	11.34 ± 0.15^{c}	-18.21 ± 0.41^{c}	-24.04 ± 0.03^{c}	18.83 ± 0.56^{c}	−25.15
3a	40.00 ± 1.94^{d}	25.00 ± 0.15^{d}	-32.24 ± 1.60^{d}	-26.08 ± 0.02^{d}	-19.89 ± 0.55^{d}	−22.46
3b	337.00 ± 1.19^{e}	2.97 ± 0.15^{d}	-7.32 ± 0.45^{e}	-20.59 ± 0.01^{e}	42.84 ± 0.19^{e}	−29.39
3c	308.00 ± 1.74^{e}	3.24 ± 0.05^{d}	-4.43 ± 0.80^{e}	-20.82 ± 0.00^{e}	52.92 ± 0.45^{f}	−30.67
4a	191.00 ± 1.67^{f}	5.23 ± 0.78^{d}	-24.70 ± 1.25^{f}	-22.05 ± 0.04^{f}	-8.55 ± 0.15^{g}	−23.60
4b	33.50 ± 0.97^{d}	29.85 ± 1.26^{e}	-28.85 ± 1.59^{f}	-26.54 ± 0.11^{d}	-7.47 ± 0.12^{g}	−33.76
4c	28.90 ± 0.44^{b}	34.60 ± 1.15^{f}	-4.52 ± 0.07^{e}	-26.92 ± 0.01^{d}	72.30 ± 0.45^{f}	−26.28
5a	180.00 ± 1.00^{f}	5.55 ± 0.25^{d}	-10.58 ± 0.45^{g}	-22.21 ± 0.01^{f}	37.53 ± 0.39^{e}	−24.56
5b	38.10 ± 0.99^{d}	26.24 ± 0.15^{e}	-17.25 ± 1.75^{c}	-26.20 ± 0.08^{d}	28.91 ± 0.35^{e}	−34.94
TOPIIα						
2a	nd	nd	nd	nd	nd	nd
2b	7.20 ± 0.15^{a}	138.89 ± 1.15^{a}	-3.01 ± 0.08^{a}	-30.49 ± 0.00^{a}	88.73 ± 1.45^{a}	−19.79
2c	35.70 ± 1.39^{b}	28.01 ± 0.45^{b}	-97.49 ± 1.35^{d}	-26.37 ± 0.01^{b}	-229.60 ± 1.10^{b}	−19.96
3a	55.70 ± 1.45^{c}	17.95 ± 0.09^{b}	-108.68 ± 1.10^{a}	-25.23 ± 0.01^{b}	-269.42 ± 1.25^{c}	−19.60
3b	1.46 ± 0.09^{d}	684.93 ± 1.35^{c}	-163.86 ± 1.45^{b}	-34.60 ± 0.01^{c}	-417.29 ± 2.39^{d}	−25.18
3c	11.70 ± 0.15^{a}	85.47 ± 0.39^{d}	-113.52 ± 1.09^{a}	-29.24 ± 0.01^{d}	-272.08 ± 1.35^{c}	−22.59
4a	2.21 ± 0.10^{d}	452.49 ± 1.45^{e}	-178.49 ± 1.49^{b}	-33.67 ± 0.01^{c}	-467.55 ± 1.39^{d}	−22.64
4b	3.37 ± 0.25^{d}	296.73 ± 1.36^{f}	-59.24 ± 1.25^{e}	-32.45 ± 0.01^{e}	-86.49 ± 1.15^{e}	−24.69
4c	nd	nd	nd	nd	nd	nd
5a	42.30 ± 1.45^{b}	23.64 ± 0.15^{b}	-3.88 ± 0.35^{c}	-25.93 ± 0.02^{b}	71.20 ± 1.05^{a}	−21.13
5b	2.81 ± 0.29^{d}	355.87 ± 0.10^{g}	-160.93 ± 1.55^{b}	-32.92 ± 0.01^{e}	-413.28 ± 1.45^{d}	−24.14

Values are expressed as mean value ± SD; n = 3; $^{a-g}$ different letters in one column or no index correspond to significant differences ($p < 0.05$); nd-not detected

while the lowest for 3b and 3c which was -20.59 kJ mol^{-1} and −20.82 kJ mol^{-}. Negative reaction entropy (ΔS) was observed for 3a, 2b, 4a and 4b, and positive for the rest of the compounds.

The tests with TOPIIα showed that 2a and 4c did not form bonds with the enzyme, while the remaining interactions were exothermic (Table 2). The highest negative change in ΔH was characterized by the interaction of the enzyme with 4a ΔH = − 178.49 kJ mol^{-1}, 3b ΔH = − 163.86 kJ mol^{-1}, 5b ΔH = − 160.93 kJ mol^{-1}, and the lowest ΔH value was recorded for 2b, ΔH = − 3.01 kJ mol^{-1} and 5a, ΔH = − 3.88 kJ mol^{-1}. K_a ranged from 684.93 to 17.95×10^3 L mol^{-1}. The highest negative ΔG was observed for 3b and it amounted -34.60 kJ mol^{-1}, and the lowest for 3a −25.23 kJ mol^{-1}. While, the reaction entropy was mostly negative, with the exception of 5a and 2a, at a level of 71.20 and 88.73 J mol K^{-1}, respectively.

Molecular docking and dynamics of propenylbenzene derivatives

The binding of an inhibitor to the active site of a protein, such as an enzyme, relies on interactions with the amino acid residues within the target domain. To investigate this, molecular docking and subsequent molecular dynamics simulations were performed for all synthesized compounds at the ATP binding region of actin's active site. The LeadFinder docking calculations indicated similar docking scores for the tested ligands ranging between approximately −5 and −8 kcal mol^{-1} for Actin. We include more detailed information in supplementary information (Fig. Sx-x + 5). To investigate further, molecular dynamics were performed, the results of which are presented in Fig. 2.

The studies showed the highest affinity for actin for 5b, amounting ΔG = − 34.94 kJ mol^{-1}, and the lowest for 2a ΔG = − 21.92 kJ mol^{-1}. This was also evident in the protein–ligand interactions observed during the MD simulations: 5b exhibited numerous and relatively stable interactions throughout the simulations (Fig. 2k). These interactions

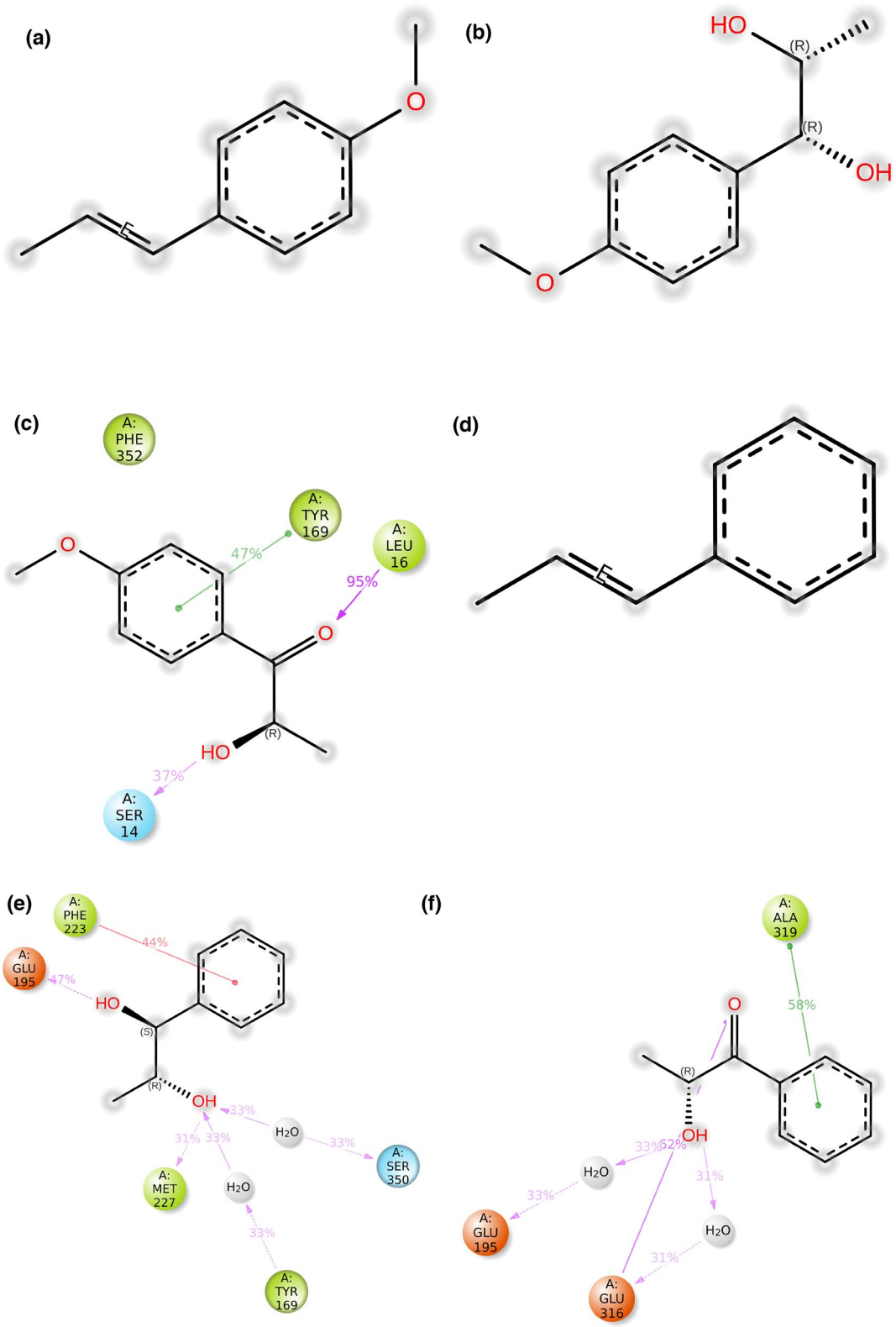

Fig. 2 2D summary of interaction diagrams of propenylbenzene derivatives–actin interactions in the active sites of actin during a 100 ns MD simulation. The hydrogen-bond interactions with residues are represented by a purple arrow directed toward the electron donor; Hydrophobic interactions are represented by a green colors, polar interactions—light blue, charged positive—navy blue ball, charged negative—red ball. **a** 3a, **b** 3b, **c** 3c, **d** 2a, **e** 2b, **f** 2c, **g** 4a, **h** 4b, **i** 4c, **j** 5a, **k** 5b. (Colour figure online)

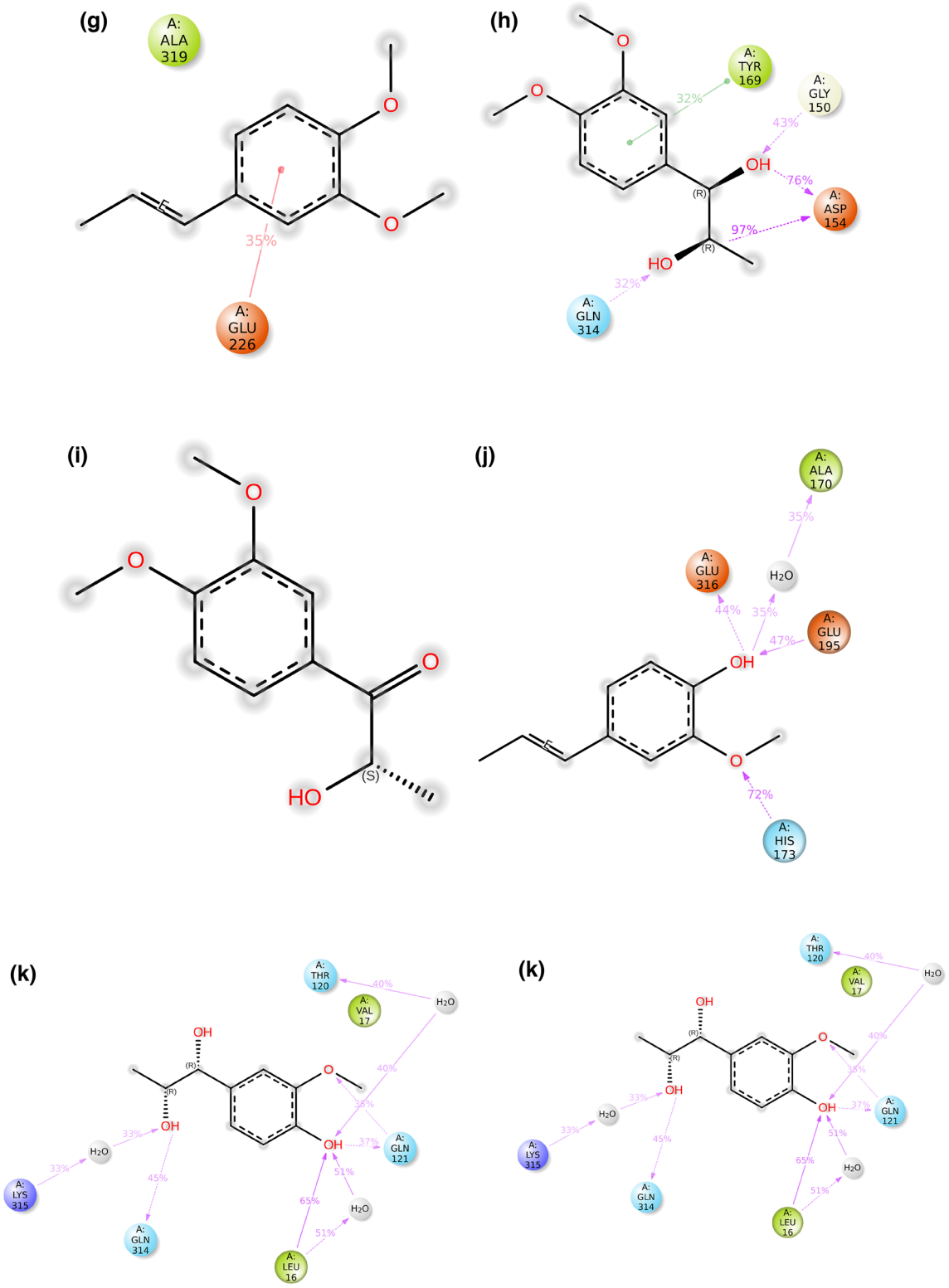

Fig. 2 (continued)

involved various residues, including LYS315, GLN314, LEU16, GLN121, VAL17, and THR120. In contrast, 2a, which demonstrated the lowest affinity, was unstable during the simulation and failed to form any significant protein–ligand interactions (Fig. 2d). The second highest affinity was observed for 4b, with a ΔG of − 33.76 kJ mol-1. The

MD simulations supported this finding, showing some long-lasting interactions with residues such as TRY169, GLY150, ASP154, and GLN314 (Fig. 2h). Notably, the interactions with ASP154 were substantial, with two polar interactions being maintained for 97% and 76% of the entire simulation time. Overall, the MD simulations seemed to correlate well with the experimental data, where compounds with many stable interactions, such as 5b and 4b. Compounds that were found to exhibit the lowest affinity did not show significant, long lasting interactions, indicating less stable binding.

Molecular docking for TOPIIα with LeadFinder indicated similar docking scores for the different compounds, ranging from − 5 to − 6.5 kcal mol^{-1}. The results of the MD simulations for TOPIIα are presented in Fig. 3. Since the experiments indicated that no stable interactions were formed for 2a and 4c were formed with TOPIIα, these compounds were omitted from the computational analysis. More detailed information about molecular docking and MD of TOPIIα is included in the supplementary data under Fig. Sx+6-11.

In the case of TOPIIα, the MD results did not accurately match the experimental data. For example, the MD simulations indicated that compounds 3b, 2c, and 4b did not form any stable interactions (Figs. 3b, e, g). While compound 2c was expected to have lower affinity, the absence of stable protein–ligand interactions for compounds 3b and 4b was unexpected, as they were measured to be the two most potent compounds in the series. Conversely, compound 5b (Fig. 3i) displayed several interactions and was found to be the third most potent compound. These discrepancies suggest that MD simulations, while useful, may not precisely model all interactions in the case of TOPIIα.

Discussion

Fight against cancer is very important at every stage of the disease and using proper supplementation can support the treatment process and also prevent metastasis. In the conducted study, it was documented that the compounds obtained from propenylbenzene by the chemo-enzymatic method, diols and hydroxy ketones, have a high antioxidant capacity, but also bind at the active site to actin and TOPIIα, the proteins important in the carcinogenesis and cancer cells migration. That indicates that diols and hydroxy ketones possess anticancer potential. The research of Contant et.al. has shown that anethole (3a) treatment (at a dose of 30 μM) shifts the proliferation of signalingpathways and increases cell apoptosis in MAP cases, NF-κB and Wnt pathways and oxidative stress [30]. The authors also proved the antioxidant potential of the compound assessed using the FRAP method and Fe^{2+}chelating activity. The 3a derivatives 3b and 3c obtained in our study showed that the compounds are very strong antioxidants. Strong antioxidative potential was also shown by 5b obtained from isoeugenol (5a). The results have high positive correlation with the reduction properties of ferrous ions. In the study of Joo et al., it was observed that supplementation of pig embryos with 3a (0.5–1 mg mL^{-1} for 6 days) had a positive effect on the activation of SHH signaling against oxidative stress [31]. Also, in the work by Bilgin et al., it has been shown that synthesized compounds based on 5a (6.25–200 μmol) strongly promoted apoptosis and inhibited the profiling and migration of human colon HT29 cells [32]. Previous studies have also shown its antimicrobial (high fungistatic activity against selected strains of *C. albicans*), antioxidant, hemolytic, and anticancer activities. The tested compounds inhibited cell proliferation of HepG2, Caco-2 and MG63 lines [14]. Therefore, we decided to verify one possible interaction that may play a role in anticancer activity.

In the carried-out experiments, all derivatives showed an exothermic reaction character confirming the occurrence of binding. The recorded energetical compensates came from the fact that the cell with tested compound in the measurement becomes warmer than the reference and then the temperature of the two cells has to be equilibrated. This creates a graph with the peaks of negative values. With successive ligand injections, the molar ratio (protein–ligand), connected with possible interactions, becomes saturated, resulting in a gradual disappearance of the peaks [33, 34]. The ITC binding curve is fitted to the binding data by integrating the injection peak area and molar ratio to ΔH (kcal mol^{-1}). In this way, the stoichiometry of the reaction (n), enthalpy (ΔH), entropy (ΔS) and binding affinity ($K_a = 1\ K_d^{-1}$) are determined [34]. The studies showed different effects of the tested compounds on actin and TOPIIα. Negative ΔH observed for all the tested compounds indicates hydrogen bonding and van der Waals interactions [34], while negative ΔS means the occurrence of hydrophobic effect and it was demonstrated for actin interacted with 3a, 2b, 4a, 4b and for TOPIIα with 3a, 3b, 3c, 2c, 4a, 4b, 5b. It could be observed that conformational changes occurred for the remaining compounds were characterized by positive ΔS [33, 34]. Actin binding was a subject of numerous studies regarding cell functions inhibition. Lu et al. showed that the Ha-VP39 nucleocapsid protein binds to actin, forming a stable complex with it preventing polymerization and F-actin formation [35]. Dhar et al. in research with curcumin confirmed similar ability of the compound to inhibit actin polymerization. Actin with curcumin bound with an affinity constant of $K_a = 2{,}45^{*}10^5$ L mol^{-1} and the affinity amounting − 34.06 kJ mol^{-1} [36]. In the studies of red clover isoflavone-actin binding, the polyphenols showed the affinity (ΔG) in the range from − 19.09 to − 16.08 kJ mol^{-1}, for biochanin A and genistein, respectively [17]. In our study, the diols and hydroxy ketones have higher ΔG in the range from − 20.59 to − 28.11 kJ mol^{-1} which demonstrates superior

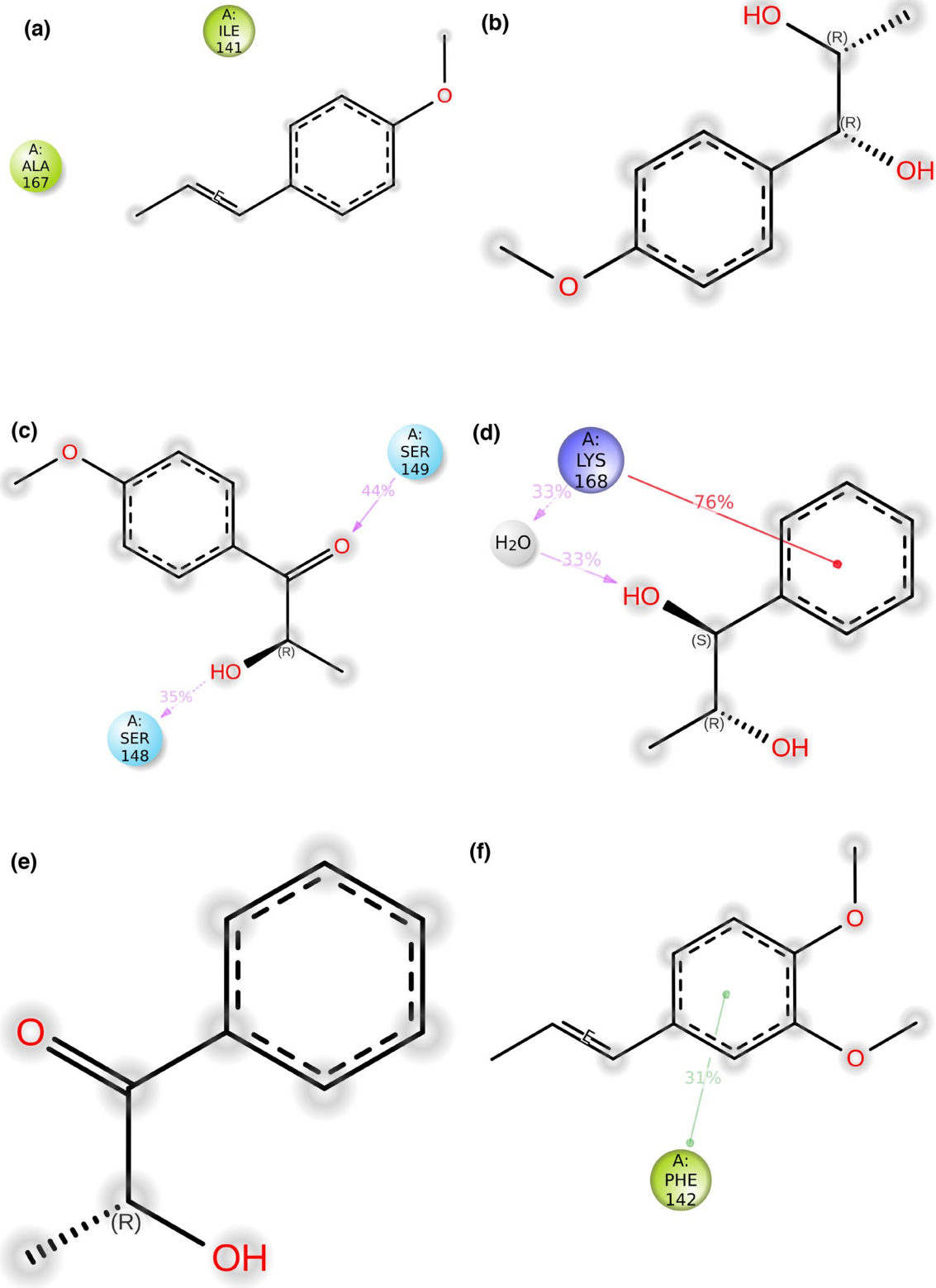

Fig. 3 2D summary of interaction diagrams of propenylbenzene derivatives-TOPIIα interactions in the active sites of TOPIIα during a 100 ns MD simulation. The hydrogen-bond interactions with residues are represented by a purple arrow directed toward the electron donor; Hydrophobic interactions are represented by a green colors, polar interactions—light blue, charged positive—navy blue ball, charged negative—red ball. **a** 3a, **b** 3b, **c** 3c, **d** 2b, **e** 2c, **f** 4a, **g** 4b, **h** 5a, **i** 5b. Note that the compounds 2a and 4c were not included since they weren't tested experimentally for TOPIIα. (Colour figure online)

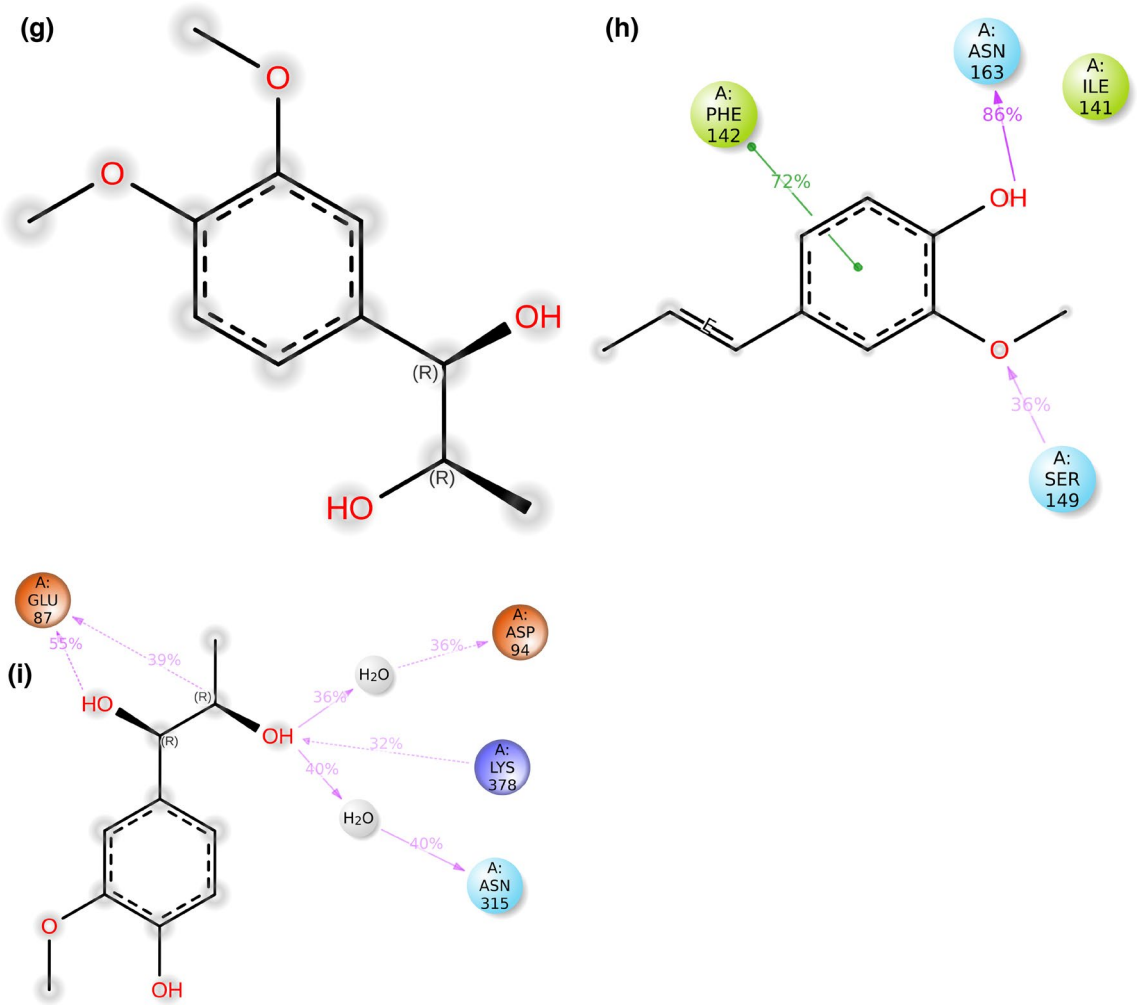

Fig. 3 (continued)

binding properties. In order to create a complementary binding site with the test compounds, negative enthalpy indicates compensation for the loss of entropy. This indicates that compounds obtained from propenylbenzene binding to permease are likely involved in the induced fit process. The ITC measurement shows that the binding of 3a, 4a and 4b, it favorably compensates for the unfavorably negative entropy. The compounds interact in a way of complementarity. The binding of compounds with actin may cause a change in the residues` chain conformation us a result of changes in the charges of individual atoms subjected non-covalent interactions. In the case of compound 2b, there was a decrease in the free energy of the considered system, as well as in negative entropy and enthalpy changes, causing compensation for the lost rotational forces and desolvation which enable adaptation of the spatial structure of the protein binding site to the ligand and its charge [37, 38].

In the case of TOPIIα, the compounds showed a higher affinity for the enzyme and a stronger binding constant as well as reaction enthalpy than in the case of actin. In a study by Dubey et al., the authors showed that nanoclusters such as AuNCs inhibit the catalytic activity of TOPIIα, the binding constant K_a was at the level of 8.39×10^4 mol^{-1}–2.59×10^5 mol^{-1} [39], higher than the propenylbenzene derivatives, although the number and the type of the interactions are also of high importance for the overall inhibiting activity. The research by Liu et al. [40] showed that the binding to TOPIIα at a unique sequence (residues: 188–238) of MDM4 inhibits the proliferation of cancer cells with K_d of 1.49 µmol [40, 41]. Negative enthalpy and negative free energy determine non-covalent interactions, mainly hydrogen bonds, ion pairs, van der Waals forces [42–44].

In our study, the affinity of results from ITC analysis and molecular docking was compared and it could be observed that the values did not exhibit consistent trends. This is a result of the different experimental assumptions, where molecular docking involves interactions only at the active site. In the case of actin, higher affinity has been

demonstrated by molecular docking, which is associated among others with endothermic conformational changes recorded during the ITC reaction. However, for the enzyme analyses, the affinity was higher in the ITC study (Table 2) which is probably a result of additional interactions outside the active site.

We investigated the experimental results using computational analysis, including molecular docking and molecular dynamics simulations. For actin, the computational results aligned well with the experiments: the highest affinity compounds exhibited more frequent and stable protein–ligand interactions compared to the least active compounds. This suggests that, in the case of actin, MD simulations can effectively model interactions and possess predictive power. However, this consistency was not observed with the computational results for TOPIIα. In this case, some of the highest affinity compounds did not form stable protein–ligand interactions, while some weaker compounds appeared to do so. The TOPIIα results indicate that a separate, more in-depth analysis must be performed to model the interactions better.

Conclusions

The results of our study showed that propenylbenzene derivatives, such as diols and hydroxy ketones, bound to actin and TOPIIα in the active sites, which was demonstrated using molecular docking, molecular dynamics and calorimetric titration. Only two compounds, 2a and 4b, did not interact with TOPIIα using ITC conditions. All obtained compounds showed high antioxidant potential in FRAP and chelating activity assays. The properties should be considered as an anti-inflammatory, antiproliferative and antimetastatic potential. The compound with the highest activity was 5b ($\Delta G = -26.20$ kJ mol^{-1} with TOPIIα and -32.92 kJ mol^{-1} with actin). As a result of the research, it was found that propenylbenzene derivatives are compounds that bind in the active site of TOPIIα. This may indicate anticancer potential, which should be continued in other research models, e.g., cytotoxicity.

Supplementary Information The online version contains supplementary material available at https://doi.org/10.1007/s10973-024-13569-8.

Author contributions Conceptualization was done by Joanna Grzelczyk and Filip Boratyński; Methodology was done by Joanna Grzelczyk, Horacio Pérez-Sánchez, Grażyna Budryn, Elisabetta Brenna and Filip Boratyński; Formal analysis and investigation were done by Joanna Grzelczyk, Jochem Nelen, Miguel Carmena-Bargueño, Ilona Gałązka-Czarnecka and Dawid Hernik; Writing—original draft preparation was done by Joanna Grzelczyk; Writing—review and editing was done by Horacio Pérez-Sánchez, Grażyna Budryn, Elisabetta Brenna and Filip Boratyński; Funding acquisition was done by Filip Boratyński; Resources was done by Dawid Hernik; Supervision was done by Filip Boratyński. The first draft of the manuscript was written by Joanna Grzelczyk, and all authors commented on previous versions of the manuscript. All authors read and approved the final manuscript.

Funding No funds, grants, or other support were received.

Declarations

Conflict of interest The authors declare that they have no known competing financial interests or personal relationships that could have appeared to influence the work reported in this paper.

Human or animal rights This article does not contain any studies with human or animal subjects.

References

1. Pandey BP, Adhikari K, Pradhan SP, Shin HJ, Lee EK, Jung HJ. In-vitro antioxidant, anti-cancer, and anti-inflammatory activities of selected medicinal plants from western Nepal. Future J Pharm Sci. 2020;6:75. https://doi.org/10.1186/s43094-020-00107-0.
2. Delam H, Bazrafshan MR, Eidi A. Thyroid cancer in the world: an epidemiological review. JHSSS. 2020;8:63–8. https://doi.org/10.30476/jhsss.2020.86850.1101.
3. Gaikwad S, Srivastava SK. Role of phytochemicals in perturbation of redox homeostasis in cancer. Antioxidants. 2021;10:83. https://doi.org/10.3390/antiox10010083.
4. Khan AQ, Rashid K, AlAmodi AA, Agha MV, Akhtar S, Hakeem I, et al. Reactive oxygen species (ROS) in cancer pathogenesis and therapy: an update on the role of ROS in anticancer action of benzophenanthridine alkaloids. Biomed Pharmacother. 2021;143:112142. https://doi.org/10.1016/j.biopha.2021.112142.
5. Okoro CO, Fatoki TH. A mini review of novel topoisomerase ii inhibitors as future anticancer agents. Int J Mol Sci. 2023;24:2532. https://doi.org/10.3390/ijms24032532.
6. Bredel M, Slavc I, Birner P, Czech T, Haberler C, Ströbel T, et al. DNA topoisomerase IIα expression in optic pathway gliomas of childhood. Eur J Cancer. 2002;38:393–400. https://doi.org/10.1016/S0959-8049(01)00387-2.
7. Liu Y, Ma J, Song J-S, Zhou H-Y, Li J-H, Luo C, et al. DNA topoisomerase II alpha promotes the metastatic characteristics of glioma cells by transcriptionally activating β-catenin. Bioengineered. 2022;13:2207–16. https://doi.org/10.1080/21655979.2021.2023985.
8. Suresh R, Diaz RJ. The remodelling of actin composition as a hallmark of cancer. Transl Oncol. 2021;14:101051. https://doi.org/10.1016/j.tranon.2021.101051.
9. Yamaguchi H, Condeelis J. Regulation of the actin cytoskeleton in cancer cell migration and invasion. Biochim Biophys Acta-Mol Cell Res. 2007;1773:642–52. https://doi.org/10.1016/j.bbamcr.2006.07.001.
10. Biber G, Ben-Shmuel A, Sabag B, Barda-Saad M. Chapter Three-Actin regulators in cancer progression and metastases: from

structure and function to cytoskeletal dynamics. Int Rev Cell Mol Biol. 2020;356:131–96. https://doi.org/10.1016/bs.ircmb.2020.05.006.
11. Brayford S, Schevzov G, Vos J, Gunning P. The role of the actin cytoskeleton in cancer and its potential use as a therapeutic target. In: Schatten H, editor. The cytoskeleton in health and disease. New York: Springer; 2015. https://doi.org/10.1007/978-1-4939-2904-7_16.
12. Zheng S, Qin F, Yin J, Li D, Huang Y, Hu L, et al. Role and mechanism of actin-related protein 2/3 complex signaling in cancer invasion and metastasis: a review. Medicine (Baltimore). 2013;102:e33158. https://doi.org/10.1097/MD.0000000000033158.
13. Olson MF, Sahai E. The actin cytoskeleton in cancer cell motility. Clin Exp Metastasis. 2009;26:273–87. https://doi.org/10.1007/s10585-008-9174-2.
14. Hernik D, Szczepańska E, Ghezzi MC, Brenna E, Włoch A, Pruchnik H, Mularczyk M, Marycz K, Olejniczak T, Boratyński F. Chemo-enzymatic synthesis and biological activity evaluation of propenylbenzene derivatives. Front Microbiol. 2023;14:1223123. https://doi.org/10.3389/fmicb.2023.1223123.
15. Oracz J, Żyzelewicz D. In vitro antioxidant activity and FTIR characterization of high-molecular weight melanoidin fractions from different types of cocoa beans. Antioxidants. 2019;8:560. https://doi.org/10.3390/antiox8110560.
16. Kalia S, Bharti VK, Giri A, Kumar B. Effect of Prunus armeniaca seed extract on health, survivability, antioxidant, blood biochemical and immune status of broiler chickens at high altitude cold deser. J Adv Res. 2017;8:677–86. https://doi.org/10.1016/j.jare.2017.08.005.
17. Budryn G, Grzelczyk J, Pérez-Sánchez H. Binding of red clover isoflavones to actin as a potential mechanism of anti-metastatic activity restricting the migration of cancer cells. Molecules. 2018;23:2471. https://doi.org/10.3390/molecules23102471.
18. Grossoehme NE, Spuches AM, Wilcox DE. Application of isothermal titration calorimetry in bioinorganic chemistry. J Biol Inorg Chem. 2010;15:1183–91. https://doi.org/10.1007/s00775-010-0693-3.
19. Stroganov OV, Novikov FN, Stroylov VS, Kulkov V, Chilov GG. Lead finder: an approach to improve accuracy of protein-ligand docking, binding energy estimation, and virtual screening. J Chem Inf Model. 2008;48:2371–85. https://doi.org/10.1021/ci800166p.
20. Madhavi Sastry G, Adzhigirey M, Day T, Annabhimoju R, Sherman W. Protein and ligand preparation: parameters, protocols, and influence on virtual screening enrichments. J Comput Aided Mol Des. 2013;27:221–34. https://doi.org/10.1007/s10822-013-9644-8.
21. Roos K, Wu C, Damm W, Reboul M, Stevenson JM, Lu C, et al. OPLS3e: Extending force field coverage for drug-like small molecules. J Chem Theory Comput. 2019;15:1863–74. https://doi.org/10.1021/acs.jctc.8b01026.
22. PubChem Sketcher V2.4 [cited 2023 July 5], Available from: pubchem.ncbi.nlm.nih.gov//edit3/index.html
23. RDKit: Open-Source Cheminformatics Software [cited 2023 July 5], Available from: www.rdkit.org
24. ChemAxon's Marvin [cited 2023 July 5], Available from: chemaxon.com/marvin
25. Grzelczyk J, Pérez-Sánchez H, Carmena-Bargueño M, Oracz J, Budryn G. Effects of *in vitro* digestion of polyphenols from coffee on binding parameters to human topoisomerase II α. Molecules. 2023;28:5996. https://doi.org/10.3390/molecules28165996.
26. Gasteiger J, Marsili M. Iterative partial equalization of orbital electronegativity—a rapid access to atomic charges. Tetrahedron. 1980;36:3219–28. https://doi.org/10.1016/0040-4020(80)80168-2.
27. Maestro Schrödinger Release 2020–4: Maestro, Schrödinger, LLC, New York, NY, 2020.
28. Schrödinger Release 2020–4: Desmond molecular dynamics system, D. E. Shaw Research, New York, NY: 2020.
29. Roos K, Wu C, Damm W, Reboul M, Stevenson JM, Lu C, Dahlgren MK, Mondal S, Chen W, Wang L, Abel R, Friesner RA, Harder ED. OPLS3e: extending force field coverage for drug-like small molecules. J Chem Theory Comput. 2019;15:1863–74. https://doi.org/10.1021/acs.jctc.8b01026.
30. Contant C, Rouabhia M, Loubaki L, Chandad F, Semlali A. Anethole induces anti-oral cancer activity by triggering apoptosis, autophagy and oxidative stress and by modulation of multiple signaling pathways. Sci Rep. 2021;11:13087. https://doi.org/10.1038/s41598-021-92456-w.
31. Joo YE, Jeong PS, Lee S, et al. Anethole improves the developmental competence of porcine embryos by reducing oxidative stress via the sonic hedgehog signaling pathway. J Anim Sci Biotechnol. 2023. https://doi.org/10.1186/s40104-022-00824-x.
32. Bilgin S, Tayhan SE, Yildirim A, Koç E. Investigation of the effects of isoeugenol-based phenolic compounds on migration and proliferation of HT29 colon cancer cells at cellular and molecular level. Bioorg Chem. 2023;130:106230. https://doi.org/10.1016/j.bioorg.2022.106230.
33. Chang JW, Armaou A, Rioux RM. Continuous injection isothermal titration calorimetry for in situ evaluation of thermodynamic binding properties of ligand–receptor binding models. J Phys Chem B. 2021;125:8075–87. https://doi.org/10.1021/acs.jpcb.1c01821.
34. Duff MR Jr, Grubbs J, Howell EE. Isothermal titration calorimetry for measuring macromolecule-ligand affinity. J Vis Exp. 2011;55:2796. https://doi.org/10.3791/2796.
35. Lu S, Ge G, Qi Y. Ha-VP39 binding to actin and the influence of F-actin on assembly of progeny virions. Arch Virol. 2004;149:2187–98. https://doi.org/10.1007/s00705-004-0361-4.
36. Dhar G, Chakravarty D, Hazra J, Dhar J, Poddar A, et al. Actin–curcumin interaction: insights into the mechanism of actin polymerization inhibition. Biochemistry. 2015;54:1132–43. https://doi.org/10.1021/bi5014408.
37. Du X, Li Y, Xia YL, Ai SM, Liang J, Sang P, Ji XL, Liu SQ. Insights into protein-ligand interactions: mechanisms, models, and methods. Int J Mol Sci. 2016;17(2):144. https://doi.org/10.3390/ijms17020144.
38. Wang X, Zheng K, Si Y, Guo X, Xu Y. Protein-polyelectrolyte interaction: thermodynamic analysis based on the titration method. Polymers. 2019;11:82. https://doi.org/10.3390/polym11010082.
39. Dubey A, Singh V, Doharey PK, Md Sk P, Samanta SK, et al. Modulating catalytic activity of human topoisomerase II α enzyme by fluorescent gold nanoclusters. Int J Biol Macromol. 2021;170:523–31. https://doi.org/10.1016/j.ijbiomac.2020.12.129.
40. Liu T, Zhang H, Yi S, Gu L, Zhou M. Mutual regulation of MDM4 and TOP2A in cancer cell proliferation. Mol Oncol. 2019;5:1047–58. https://doi.org/10.1002/1878-0261.12457.
41. Tavakoli N, Ghalandari B, Badalkhani-Khamseh F, Ding X, Divsalar A. Molecular dynamics simulation study on the effect of oxali-palladium as a catalytic inhibitor of human topoisomerase IIα. Iran J Sci Technol Trans Sci. 2022;46:1575–82. https://doi.org/10.1007/s40995-022-01384-5.
42. Gutiérrez-Climente R, Prost E, Cordin A, Chesta C, Duma L. Isothermal calorimetry: molecular interactions between small molecules in organic solvents. Appl Calorim. 2022. https://doi.org/10.5772/intechopen.104756.
43. Su H, Xu Y. Application of ITC-based characterization of thermodynamic and kinetic association of ligands with proteins in drug design. Front Pharmacol. 2018;9:1133. https://doi.org/10.3389/fphar.2018.01133.

44. Ladbury JE. Application of isothermal titration calorimetry in the biological sciences: things are heating up! Biotechniques. 2004;37(6):885–7. https://doi.org/10.2144/04376TE01.